

Entanglement Scaling of Fractional Quantum Hall states through Geometric Deformations

Andreas M. Läuchli, Emil J. Bergholtz, and Masudul Haque

Max-Planck-Institut für Physik komplexer Systeme, Nöthnitzer Straße 38, D-01187 Dresden, Germany

E-mail: aml@pks.mpg.de, ejb@pks.mpg.de and haque@pks.mpg.de

Abstract. We present a new approach to obtaining the scaling behavior of the entanglement entropy in fractional quantum Hall states from finite-size wavefunctions. By employing the torus geometry and the fact that the torus aspect ratio can be readily varied, we can extract the entanglement entropy of a spatial block as a continuous function of the block boundary length. This approach allows us to extract the topological entanglement entropy with an accuracy superior to what is possible on the spherical or disc geometry, where no natural continuously variable parameter is available.

Other than the topological information, the study of entanglement scaling is also useful as an indicator of the difficulty posed by fractional quantum Hall states for various numerical techniques.

PACS numbers: 73.43.Cd, 03.67.-a, 71.10.Pm

1. Introduction

Describing condensed matter phases using entanglement quantifiers from quantum information theory is a rapidly growing interdisciplinary topic [1, 2]. Of special interest are the relatively rare cases where entanglement can provide information not readily captured by conventional quantities such as correlation functions. This is the situation for systems possessing *topological order* [3], where entanglement considerations have proven useful [4, 5, 6]. In particular this has led to insight into the structure of fractional quantum Hall (FQH) states [7, 8, 6, 9, 10, 11, 12, 13, 14]. In this Article we focus on entanglement in this most realistic class of topologically ordered states.

A prominent measure of entanglement is the von Neumann entropy of entanglement, S_A , measuring the entanglement between a block (A) and the rest (B) of a many-particle system in a pure state. The entanglement entropy $S_A = -\text{tr}[\rho_A \ln \rho_A]$ is defined in terms of the reduced density matrix, $\rho_A = \text{tr}_B \rho$, obtained by tracing out B degrees of freedom from the system density matrix $\rho = |\psi\rangle\langle\psi|$, with $|\psi\rangle$ denoting a ground state wave function. In one dimension the scaling behavior of the block entanglement entropy is well understood, see, *e.g.*, Ref. [2]. In two dimensions (2D), no such generic classification exists. However, for topologically ordered states in two dimensions, the entanglement entropy contains topological information about the state: S_A scales as

$$S_A = \alpha L - n\gamma + \mathcal{O}(1/L), \quad (1)$$

where L is the block boundary length, γ characterizes the topological field theory describing the state [4, 5], while n counts the number of disconnected components of the boundary. The value of γ is related to the “quantum dimensions” of the quasiparticle types of the theory, $\gamma = \ln \mathcal{D}$, where \mathcal{D} is the total quantum dimension. For Laughlin states at filling $\nu = 1/m$, $\gamma = \frac{1}{2} \ln m$. For more intricate FQH states, some examples of γ values are provided in Refs. [4, 15, 8]. If γ can be determined accurately, its value can in principle be used to determine whether a topological phase belongs to the universality class of a given topological field theory.

A numerical determination of γ and α requires information about S_A for a number of different boundary lengths, L . In Ref. [7] such information was obtained from finite-size FQH wavefunctions by approximating the spatial partitioning by partitioning of the discrete set of Landau level orbitals. Refs. [7, 8, 10] used spherical geometries, and explored ways of extrapolating entanglement information from such geometries to the thermodynamic limit. Ref. [12] used disk geometries to calculate γ for bosonic FQH wavefunctions. The accuracy in the determination of γ from finite-size wavefunctions on these geometries remains disappointing (10%–30% for the simplest Laughlin states). Improved methods for calculating γ are thus sorely needed.

In this work, we report a significant advance in this direction, through the use of the torus geometry and the fact that the aspect ratio (circumference) of the torus can be varied continuously without drastically altering the torus setup or symmetry. Varying the circumference changes the length of the boundary between A and B . No natural analogous continuous parameter exists in the other geometries, so that in those cases

each system size and bipartition provides only one point in parameter space. Exploiting the continuous parameter, we present a procedure that leads to an accuracy in γ down to a few percent. Our analysis also provides a visual and physical indication of the reliability of the extracted γ value.

Previously, Ref. [16] reported a naïve modification of the sphere algorithm of Ref. [7] to the torus geometry with fixed aspect ratio. We will show why this analysis was inappropriate and based on an extrapolation procedure that is not meaningful for the torus geometry.

In addition to the topological content of the subleading term in (1), the dominant linear term itself is also of some importance. The rate of entanglement growth, α , indicates how challenging the state is to simulate on a classical computer, through a one-dimensional algorithm like DMRG [17, 18], or through recently-proposed true two-dimensional algorithms like PEPS [19] or MERA [20]. DMRG has been used to simulate FQH states [21, 22, 23, 24], and these states pose a future challenge for two-dimensional algorithms currently under development.

The calculation of the topological entanglement entropy γ is of significant current interest, not only for FQH states but also for various other topologically ordered states. For the zero-temperature Kitaev model, it is relatively easy to calculate γ ; so the concept has been used in exploring issues such as temperature effects and quantum phase transitions [25, 26, 27, 28]. For quantum dimer models and related states, considerations of entanglement scaling are more intricate [29, 30], of difficulty comparable to FQH states. More generally, entanglement scaling in 2D states of all kinds has become the focus of intense study at present [31, 2, 32].

In Section 2 we show how the torus geometry allows us to map the interacting Landau level (LL) problem onto a one-dimensional lattice model, appropriate for studying bipartite entanglement. In Section 3 we outline the general behavior of entanglement entropy on the torus geometry and deal with the issue of torus degeneracies. In Section 4 we present our main results, including an analysis leading to the determination of γ . The concluding Section 5 connects to the existing literature and discusses implications of our results.

2. Torus setup – geometry, partitioning

We study an N -electron system on a torus (see Fig. 1) with periods L_1, L_2 in the x - and y -directions, satisfying $L_1 L_2 = 2\pi N_s$ in units of the magnetic length. The integer $N_s = N/\nu$ is the number of magnetic flux quanta. In the Landau gauge, $\mathbf{A} = By\hat{\mathbf{x}}$, a basis of single particle states in the lowest Landau level can be taken as

$$\psi_j = \pi^{-1/4} L_1^{-1/2} \sum_m e^{i(\frac{2\pi}{L_1} j + mL_2)x} e^{-(y + \frac{2\pi}{L_1} j + mL_2)^2/2} \quad (2)$$

with $j = 0, 1, \dots, N_s - 1$. The states ψ_j are centered along the lines $y = -2\pi j/L_1$. Thus the y -position is given by the x -momentum j .

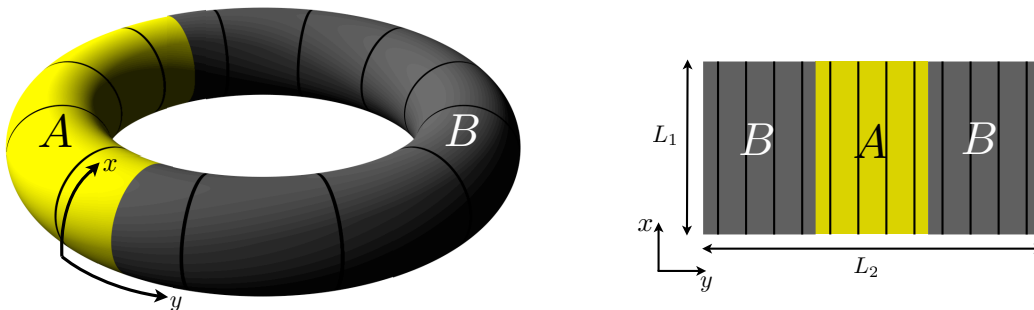


Figure 1. Geometry of the torus and bipartitioning. The lowest Landau level is spanned by orbitals which in the Landau gauge are centered along the circles shown. On the right, we represent the torus as a rectangular region with periodic boundary conditions in both directions. The dimensions of this rectangle (L_1 , L_2) are the two circumferences of the torus. The example shown here has $N_s = 12$ orbitals with $l_A = 4$ orbitals in the A block.

A generic translation-invariant two-body interaction Hamiltonian, acting within a Landau level, can be written as

$$H = \sum_n \sum_{k>|m|} V_{km} c_{n+m}^\dagger c_{n+k}^\dagger c_{n+m+k} c_n \quad , \quad (3)$$

where c_m^\dagger creates an electron in the state ψ_m and V_{km} is the amplitude for two particles to hop symmetrically from separation $k+m$ to $k-m$ [33]. Hence, the problem of interacting electrons in a Landau level maps onto a one-dimensional, center-of-mass conserving, lattice model with lattice constant $2\pi/L_1$. This provides a natural setting for defining entanglement, by bipartitioning the system into blocks A and B , which consist respectively of l_A consecutive orbitals and the remaining $l_B = N_s - l_A$ orbitals (Fig. 1). Since the orbitals are localized in the direction of the lattice, this is a reasonable approximation to spatial partitioning, as on the sphere [7, 8, 6, 10, 11].

Because this partitioning implies two disjoint edges between the blocks, each of length L_1 , the entanglement entropy should satisfy the following specific form of (1):

$$S_A(L_1) = 2\alpha L_1 - 2\gamma + \mathcal{O}(1/L_1). \quad (4)$$

Thus our setup should yield a linear scaling form of the entropy with the $L_1 = 0$ intercept at -2γ .

In this work, we obtain ground states of (3), in the orbital basis (2) using the Lanczos algorithm for numerical diagonalization. We study bipartite entanglement in these ground states. Apart from diagonalizing the Coulomb problem we also consider pseudopotential interactions [34, 35] which have the Laughlin states [36] as exact ground states. The largest Hilbert space sizes considered are 208'267'320 for 39 orbitals at $\nu = 1/3$, 19'692'535 for 45 orbitals at $\nu = 1/5$ and 66'284'555 for 35 orbitals at $\nu = 2/5$. The simulations are however currently limited by the size of the reduced density matrices to be calculated and fully diagonalized.

Fractional quantum Hall states have degenerate ground states on the torus geometry. It is convenient to label the ground states by their corresponding thin torus (or Tao-Thouless, TT) patterns [33, 37, 38, 39, 40]. For example, for $\nu = 1/3$ there are three degenerate states, which correspond to the TT configurations

$$\begin{array}{l}
 100100100 \left| 100100100100100100 \right| 100100100 \\
 010010010 \left| 010010010010010010 \right| 010010010 \\
 001001001 \left| \underbrace{001001001001001001}_{A} \right| 001001001 ,
 \end{array} \tag{5}$$

for $N_s = 36$. Here the positions of 1's indicate the positions (or, equivalently, the transverse momenta) of filled single particle states. An equal partitioning ($l_A = l_B = N_s/2$) is illustrated.

In general, abelian FQH states at $\nu = p/q$ have q degenerate ground states, related to each other through translation and corresponding to q thin-torus patterns, each composed of unit cells with p electrons on q sites. These states are ground states for generic (two-body) interactions as $L_1 \rightarrow 0$ [33]. For non-abelian states there is an enhanced degeneracy and the corresponding thin torus patterns are not simply translations of each other.

The thin torus states are unentangled product states, in the orbital basis. As L_1 is increased from zero, fluctuations on top of the TT states will make the states entangled. A crucial property of the FQH states is that their bulk versions are, for appropriate interactions, adiabatically connected to their respective TT states and the gap is finite for all L_1 [33, 37]. This allows us to probe the response of these states as the geometry is deformed. Such deformations have also been considered to extract properties such as the Hall viscosity [41, 42], to put consistency conditions of FQH states [43], to find instabilities to competing states (see *eg* [44, 45]) and to deform the torus to the solvable thin torus limit as discussed above. All the three fractions studied in this paper ($\nu = 1/3, 1/5$, and $2/5$) are, for the pseudopotential as well as the Coulomb interactions, continuously connected to their TT states.

3. Degeneracy averaging, Area law at constant L_1

For any finite L_1 the charge density modulations of the TT pattern will prevail to some extent, leading to different entanglement in the q degenerate ground states. We illustrate this in Fig. 2(a) where we plot the entanglement entropy $S_A(l_A)$ as a function of l_A in the three degenerate $\nu = 1/3$ Laughlin wave functions. For each l_A two out of the three entanglement entropies are equal, while the third one is different, as can be inferred from examining the partitionings shown in Equation (5). Two of the TT patterns have 1-0 and 0-1 cuts at the block boundaries, while the third has only 0-0 cuts. Since the microscopic environment at the two boundaries determines the entanglement spectrum [13] and hence the entanglement entropy, this implies that two of the entanglement entropies are equal at each l_A .

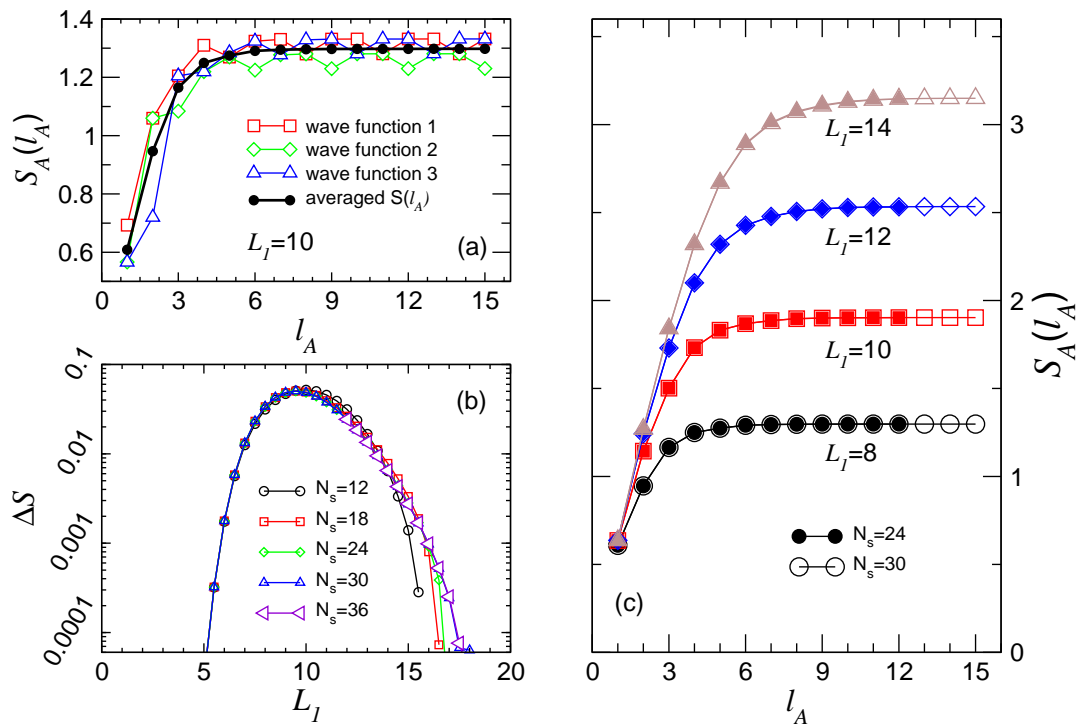


Figure 2. Degeneracy averaging and l_A dependence. (a) Entanglement entropy in different degenerate sectors for the $\nu = 1/3$ Laughlin state, and their arithmetic average. (b) difference between degeneracy-averaged S_A and largest individual-sector S_A , as a function of L_1 . They differ significantly only for intermediate L_1 . (c) Degeneracy-averaged S_A versus l_A , for different L_1 values.

The $S_A(l_A)$ each have prominent oscillatory behavior. However, we find that the *arithmetic mean* of the three individual entanglement entropies is remarkably free of oscillations. We will thus base all our following discussions on the degeneracy-averaged entropy \ddagger . Ultimately this averaging will become unimportant for very large L_1 , as Fig. 2(b) shows that the difference ΔS between the maximum and the mean entanglement entropies in the q sectors vanishes rapidly at large L_1 (starting to decrease after $L_1 \sim 10$ in the Laughlin $\nu = 1/3$ case shown).

In Fig. 2(c) we study the l_A and N_s dependence for a given L_1 . At constant L_1 we expect the entropy to saturate once l_A is large enough, since the block boundary length ($2L_1$) is held constant. This is indeed what is found numerically in Fig. 2(c). The length scale controlling the saturation is the (real space) correlation length ξ_r in the y direction of the incompressible FQH liquid. The correlation length ξ_o measured in number of orbitals is expected to scale as $\xi_o \sim \xi_r \times L_1/2\pi$. The saturation of the entanglement entropy for large l_A is in complete analogy to the area law for one-dimensional gapped systems [46, 47]. It is this saturation value $S_A(L_1)$ of the entanglement entropy obtained

\ddagger In principle the averaging could be done in other ways, for example, one could average over the density matrices $\rho \rightarrow \sum_{i=1}^{N_{GS}} \rho^{(i)}/N_{GS}$ or reduced density matrices, and then compute the entanglement entropy from this averaged matrix. We do not however pursue such alternate averaging procedures in the present work.

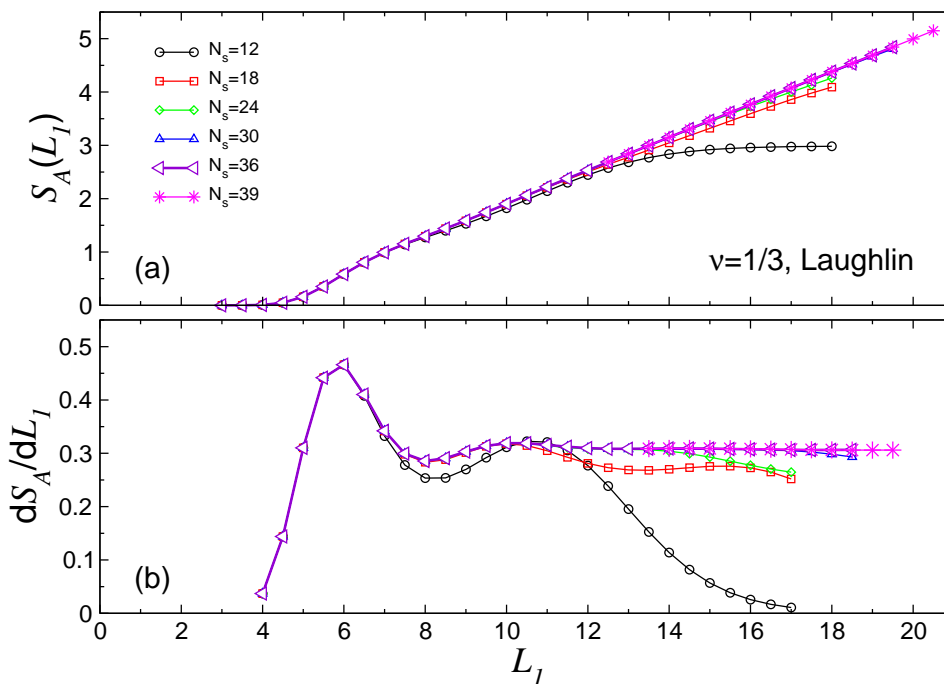


Figure 3. $\nu = 1/3$ Laughlin state: Entanglement entropy, (a) S_A and (b) its derivative dS_A/dL_1 for the Laughlin state at $\nu = 1/3$ as a function of L_1 . From the plateau behavior in dS_A/dL_1 for $L_1 \gtrsim 12$ we infer $\alpha \approx 0.153(2)$.

for $l_A \gg \xi_o$ that will be analyzed in the following. To avoid the finite size effect as far as possible we consider $l_A = N_s/2$ for N_s even, and $l_A = (N_s - 1)/2$ for N_s odd, in the rest of this article. From Fig. 2(c) we can again infer that the averaged S_A indeed has a much smoother dependence on the block size compared to the S_A for the individual degenerate states.

4. Accessing the scaling regime

In this Section we provide our main numerical results and discuss how α and γ can be extracted by continuously varying L_1 . As mentioned above, from now on S_A refers to the equal-partitioning entanglement entropy ($l_A = N_s/2$ for N_s even, and $l_A = (N_s - 1)/2$ for N_s odd).

$\nu = 1/3$ Laughlin state — Fig. 3 shows the behavior of $S_A(L_1)$ (a) and its derivative dS_A/dL_1 (b), for the Laughlin state at fraction $\nu = 1/3$, arguably the most prominent and also the simplest FQH state. In this figure and subsequently, we use a five-point formula to numerically obtain derivatives. The entanglement entropy $S_A(L_1)$ remains minuscule until $L_1 \sim 3$, and then gradually changes to the expected linear increase behavior which is reached around $L_1 \sim 7$. There are oscillations on top of the linear behavior, which are more prominent in the derivative plot (b). The oscillations can be interpreted as an interplay between the finite circumference along the x direction (finite

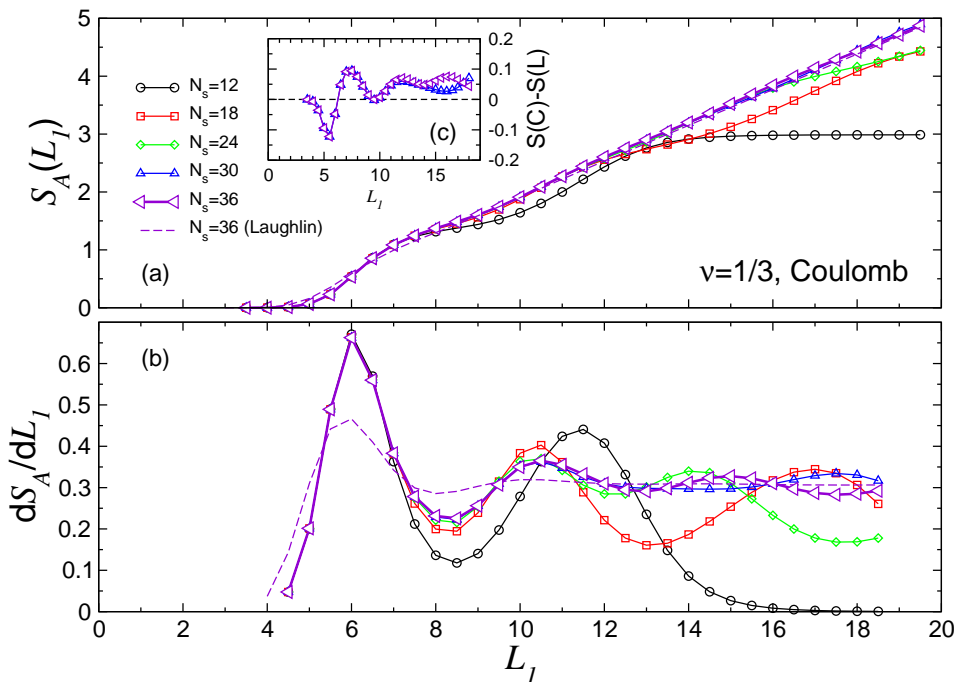


Figure 4. $\nu = 1/3$ Coulomb ground state: Entanglement entropy, (a) S_A and (b) its derivative dS_A/dL_1 for the Coulomb ground state at $\nu = 1/3$ as a function of L_1 . One curve for the Laughlin state is also shown for comparison (dashed line). In the inset (c) the difference in $S_A(L_1)$ between the Coulomb and the Laughlin is displayed (for $N_s = 30, 36$).

L_1) and the interparticle distance. The oscillations die off as a function of L_1 , so that if N_s is large enough one can get the scaling form at large L_1 .

For small L_1 the finite size convergence is essentially perfect. At larger L_1 , the $S_A(L_1)$ and dS_A/dL_1 curves show stronger dependence on N_s . The N_s -dependence shows up first for the smallest system sizes and at increasing L_1 for progressively larger system sizes. This reflects the fact that, for any finite-size system, at very large L_1 the edges of A get too close (small L_2) and cannot be thought of as independent [13]. In particular, once L_1 exceeds some value we enter the “dual thin torus” or “thick torus” limit [40, 48, 43], and the entanglement entropy levels off to some saturation value. Corresponding to the saturation of $S_A(L_1)$, the derivative dS_A/dL_1 drops off to zero after some L_1 .

Thus, the scaling form of (4) is valid only in a window of L_1 , after the oscillations have subsided but before $S_A(L_1)$ saturates, or shows other precursor finite size effects. This plateau region can be seen clearly in the dS_A/dL_1 curve for the $\nu = 1/3$ Laughlin data for $L_1 \gtrsim 12$. The finite size convergence of the data also provides a clear signal showing whether the bulk scaling regime is reached or whether (geometrical) finite size effects are still significant in the numerically accessible L_1 regime.

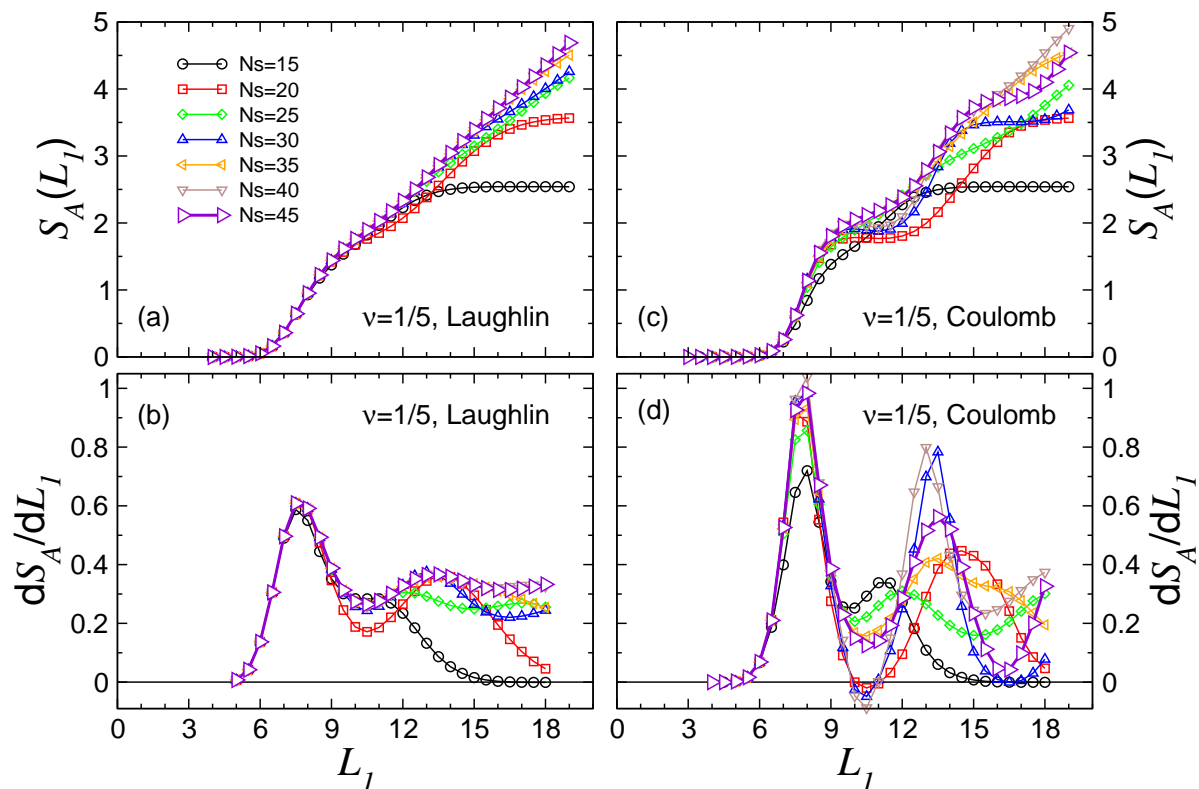


Figure 5. $\nu = 1/5$ **Laughlin vs Coulomb:** Entanglement entropy (a) and its derivative (b) for the $\nu = 1/5$ Laughlin wave functions. Entanglement entropy (c) and its derivative (d) for the $\nu = 1/5$ Coulomb ground state.

$\nu = 1/3$ *Coulomb ground state* — Fig. 4 plots (a) $S_A(L_1)$ and (b) dS_A/dL_1 for the Coulomb ground states at $\nu = 1/3$. While this state has somewhat more severe finite-size effects and oscillatory behaviors compared to the model Laughlin state of Fig. 3, we note that the scaling form of their entanglement entropies are very similar. To further highlight this fact we plot the difference between the entanglement entropies as a function of L_1 in the inset of Fig. 4(c). The similarity of entanglement entropies of the two states is not unexpected from the perspective that the states have a large overlap for all L_1 [45], but it is nevertheless interesting considering that a more “generic” state such as the Coulomb state is expected to have larger entanglement. One could thus have expected the Coulomb state to have a larger α , as defined in Eq. 1, but Fig. 4(b) suggests a very similar $\alpha \approx 0.15(1)$.

$\nu = 1/5$ — Fig. 5 shows the $S_A(L_1)$ and dS_A/dL_1 behaviors at $\nu = 1/5$, for both the Laughlin (a) & (b) and the Coulomb ground state (c) & (d). As expected, the finite-size oscillations are much more severe in these states. This is expected as the interparticle distance is larger; thus larger systems should be required to reach the scaling regime. Moreover, the proximity to the Wigner crystal phase makes the Coulomb ground state deviate more substantially from the Laughlin state than is the case at $\nu = 1/3$ [49, 45]. While we are able to get an almost N_s -converged $S(L_1)$ curve up to $L_1 \sim 18$ for the

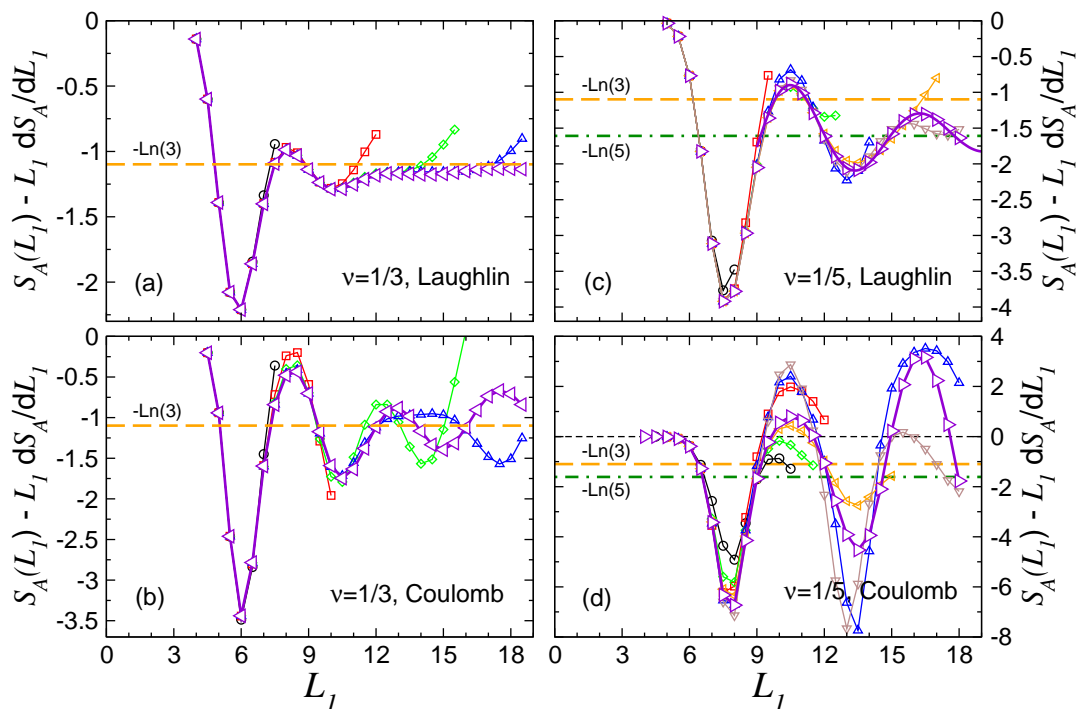


Figure 6. L_1 -local extraction of γ . The intercept of local linear approximations to the $S_A(L_1)$ curves, *i.e.*, $S_A(L_1) - L_1 \times dS/dL_1$, plotted as a function of L_1 . In the scaling regime, this quantity should give -2γ . The symbols for $\nu = 1/3$ ($\nu = 1/5$) are the same as in Fig. 4 (Fig. 5). Theoretically expected -2γ values are shown as dashed horizontal lines. In panel (c) the solid line through the largest size data is the fit obtained using Equation (6).

Laughlin state [leading to a rough estimate of $\alpha \approx 0.17(2)$], the finite size effects in the Coulomb ground state are so severe that no meaningful extraction of α is possible with current system sizes.

Extraction of the topological entanglement entropy γ — In Fig. 6 we show calculations of γ for the Laughlin state at $\nu = 1/3$ (a) and $\nu = 1/5$ (c) as well as for the Coulomb ground state at the same fractions (b) & (d). Evaluating the L_1 derivative using a centered 5-point formula, we plot $S_A(L_1) - L_1 \times dS/dL_1$ as a function of L_1 . This quantity is the intercept of a linear approximation made to the $S_A(L_1)$ curve locally at each L_1 . It should take the value -2γ in the scaling region, see Equation (4). Not surprisingly, the intercept oscillates at intermediate L_1 , has a plateau in the “scaling window” described above, and then moves off to a large positive value when L_1 is yet larger entering the thick torus regime. The plateau region value gives us the best estimate for the topological entanglement entropy. A significant advantage of our analysis is that, by examining the dS_A/dL_1 curve (and its N_s dependence), we can identify the correct window of L_1 values to use.

In Fig. 6(a) the $\nu = 1/3$ Laughlin shows such a clear plateau region. The plateau region value around $L_1 \sim 18$ gives us the best estimate for the topological

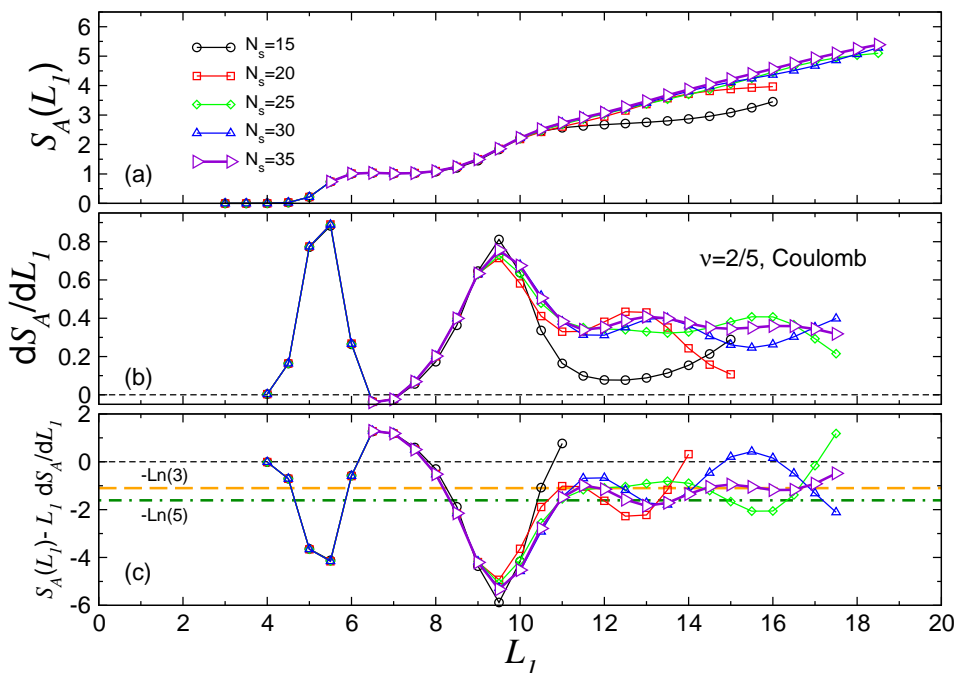


Figure 7. $\nu = 2/5$ Coulomb ground state. (a) S_A and (b) its derivative dS_A/dL_1 for the Coulomb ground state at $\nu = 2/5$ as a function of L_1 . (c) Estimation of -2γ through a plot of the L_1 -local intercept against L_1 .

entanglement entropy $\gamma \approx 0.565(5)$, to be compared to the theoretical expectation $\gamma = \ln(3)/2 \approx 0.5493$. The difference amounts to only 3 percent in this ideal case.

For the $\nu = 1/5$ Laughlin [Fig. 6(c)], the finite-size issues are significantly larger, and the oscillations have not yet damped out at accessible sizes. However, one can take the average of the oscillating values to get a reasonable estimate of γ . We use a simple damped oscillation fitting ansatz of the form:

$$f(L_1) = -2\gamma + a \times \exp[-bL_1] \times \sin(cL_1 - d), \quad (6)$$

and fit the $N_s = 45$ curve for $L_1 > 9$, yielding an estimate of $\gamma \approx 0.81$. This value again compares very favorably to the theoretical expectation $\gamma = \ln(5)/2 \approx 0.8047$.

At each of these fractions, the finite-size convergence is worse for the Coulomb ground state compared to the Laughlin ground state. While for the $\nu = 1/3$ Coulomb [Fig. 6(b)] a fitting analysis along the lines of the $\nu = 1/5$ Laughlin still provides a reasonable γ estimate: $\gamma \approx 0.60$, the $\nu = 1/5$ Coulomb state [Fig. 6(d)] clearly does not allow a meaningful γ extraction from system sizes presently reachable through numerical exact diagonalization.

$\nu = 2/5$ Coulomb interaction — Finally, in Figure 7 we consider the Coulomb ground state at filling $\nu = 2/5$, whose γ value has not been studied numerically so far. This state is, for all L_1 , well described by the torus version [50] of the Jain [51] (or, equivalently, the hierarchy [34]) state. The finite-size effects are somewhat less severe than the $\nu = 1/5$ Coulomb case [Figs. 5(c,d) and 6(d)]. One obtains an entanglement growth rate of

$\alpha \approx 0.188(16)$. While the N_s -convergence is not good enough for a precise determination of γ (expected to be $\frac{1}{2} \ln 5$), examination of the largest two available sizes suggests that two or three additional sizes may be enough to provide an estimate at the $\sim 10\%$ accuracy level.

5. Discussion

In this article we have shown how continuous geometric deformations of the torus can be employed to explore the scaling form of the entanglement entropy. This has allowed us to propose a method for determining the topological part, γ , from finite-size wavefunctions, to greater precision compared to earlier analyses which did not utilize any continuous parameter. Our analysis indicates that current state-of-the-art system sizes are enough to obtain reliable γ calculations for the simplest fractional quantum Hall states (Laughlin states), but that more intricate states would require larger sizes than currently accessible, in order to reach the scaling limit. Our procedure provides a clear method for identifying whether the scaling window has been reached or not.

There has been an earlier report of entanglement entropy and γ calculations on the torus [16], using fixed aspect ratio, $L_1/L_2 = 1$. Ref. [16] performed $N_s \rightarrow \infty$ extrapolations at fixed l_A , and expected the extrapolated values to scale as $c_1 \sqrt{l_A} - 2\gamma$. We illustrate such a fixed l_A extrapolation in Fig. 8. The extrapolation does not lead to a physically meaningful limit because the boundary lengths diverge and the two boundaries get infinitesimally close to each other, in the $N_s \rightarrow \infty$ limit.

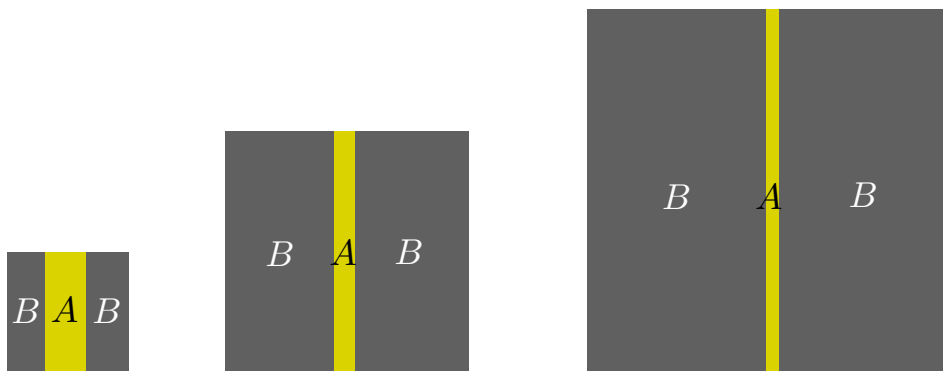


Figure 8. Extrapolation at fixed aspect ratio and fixed l_A . Fixed l_A implies that the area covered by the region A is constant. Such extrapolation does not lead to a well-defined limit as the limiting case is one with infinitesimal thickness and infinite boundary length.

The extrapolation of Ref. [16] arose from an incorrect adaptation of the procedure of Ref. [7] which was designed for the sphere geometry. For the spherical case, the

fixed- l_A extrapolation takes one to the well-defined limit of an infinite disk with circular A region, where the boundary length indeed scales as $\sim \sqrt{l_A}$. Also for the disk [12], the fixed- l_A extrapolation to $N \rightarrow \infty$ is well-defined as the limiting situation is again an infinite disk with constant density. (The density is not constant in finite-size disk simulations.) However, for the torus with unit aspect ratio, the fixed- l_A extrapolation to $N \rightarrow \infty$ has a pathological limit for the shape of the A block, and the limiting entanglement entropy has no reason to scale as $\sim \sqrt{l_A}$. A plot of the extrapolated S_A versus $\sqrt{l_A}$ thus has no obvious connection to the entropy scaling as a function of the boundary length, or to the definition of γ as formulated in Refs. [4, 5].

The idea of obtaining entanglement entropy scaling through varying discrete torus circumferences has been employed in Ref. [29] for the dimer model on the triangular lattice. The details are quite different from the FQH case. It is possible that some of the ideas developed here for the FQH context might be transferred fruitfully to numerical work on dimer models or other lattice models. Ref. [32] has studied entanglement of *integer* quantum Halls states on a torus, between true spatial partitions rather than orbital partitions. The orbital partitioning entanglement is zero for integer quantum Hall states because they are product states in the orbital basis.

Since Ref. [7, 8] reported entanglements of the same Laughlin states on a different geometry, it is interesting to compare the magnitudes of the entanglement entropy. The data tabulated in Ref. [8] for the $\nu = 1/3$ state yields a value of $\alpha \sim 0.15$, which is close to that obtained from the torus entanglement data reported in this work. While this is not unexpected, it has several instructive implications. First, it can be regarded as additional evidence that orbital partitioning entanglement is a good approximation to spatial partitioning entanglement. Second, it shows that the entanglement entropy contributions from the two edges simply add for a block with two edges compared to one edge.

In addition, the fact that the sphere and the torus have the same “entanglement entropy density” per unit boundary length, allows us to compare the difficulty of DMRG simulations on spherical and toroidal geometries based on considerations of linear sizes alone. Conventional wisdom might be that the torus is significantly more difficult to treat using DMRG, because it is a system with periodic boundary conditions while the sphere is more analogous to a lattice system with open boundary conditions. However, the torus has the same block boundary length everywhere ($2L_1 = 2\sqrt{2\pi N_s}$ for the hardest case of unit aspect ratio), while the block boundary on a sphere varies. For DMRG on a spherical geometry, the dominant reduced entropy contributions comes from the equator region, where the block boundary is $L = \pi\sqrt{2N_s}$. The torus boundary is only a factor $2/\sqrt{\pi} \approx 1.13$ larger than the sphere case, rather than being twice as large. Moreover, from the two edges one benefits twice the (negative) contribution from the topological part of the entanglement entropy (in contrast to a single contribution on the sphere). We therefore infer that DMRG on the torus geometry is not as drastically more difficult compared to the sphere case, as would be suggested by the argument of two block boundaries versus one.

The entanglement entropy S in a bipartition of a quantum state puts a lower bound on the number of states m to be kept in an accurate DMRG simulation through the relation $m \sim \exp(S)$. The computational complexity of DMRG being polynomial in m , the scaling of S with system geometry is thus of primary importance. In the simplest cases, *e.g.*, one dimensional gapped quantum systems with local interactions, the entropy S does not depend on the block length, enabling DMRG simulations for basically infinite systems at constant m . Torus FQH simulations at *constant* L_1 [22] also belong to this tractable class. If one is however interested in describing true bulk FQH systems at fixed aspect ratio ($L_1/L_2 = \text{const}$), then entropy S will scale linearly with $L_1 \propto \sqrt{N_s}$. This translates into $m \propto \exp[\text{const} \times \sqrt{N_s}]$, i.e., accurate DMRG simulations for bulk FQH states scale exponentially in the physical width, similar to 2D lattice models [18].

The present work opens up a number of directions deserving exploration. Our analysis provides a way to decide on whether or not available wavefunction sizes provide access to the entanglement scaling regime. Thus, as bigger wavefunctions become available, our analysis can be applied directly to obtain better calculations of the topological entanglement entropy γ . Eventually, this type of calculation could become a standard tool for diagnosing unknown or poorly-understood FQH states. Another obvious direction is the study of entanglement scaling through geometric deformations at other fractions and more complicated states. It may also be interesting to try to devise continuous geometric tuning parameters for other geometries, *e.g.*, one may consider ellipsoidal geometries as deformations of the sphere, although setting up the Landau level problem in such geometries is not straightforward or convenient. It is possible that a combination of various deformation considerations might lead to further refined procedures for estimating entanglement scaling and γ .

6. Acknowledgments

We thank Kareljan Schoutens for suggesting entanglement calculations on the torus with varying geometry, and Juha Suorsa for collaboration on related topics. MH thanks Nicolas Regnault for related discussions. We acknowledge MPG RZ Garching and ZIH TU Dresden for allocation of computing time.

References

- [1] L. Amico, R. Fazio, A. Osterloh, and V. Vedral, *Rev. Mod. Phys.* **80**, 517 (2008)
- [2] J. Eisert, M. Cramer, M.B. Plenio, *Rev. Mod. Phys.* **82**, 277 (2010).
- [3] X. G. Wen and Q. Niu, *Phys. Rev. B* **41**, 9377 (1990); X. G. Wen, *Phys. Rev. B* **40**, 7387 (1989), *J. Math. Phys.* **4**, 239 (1990); X. G. Wen, *Quantum Field Theory of Many-body Systems*, (Oxford, 2004); M. Oshikawa and T. Senthil, *Phys. Rev. Lett.* **96**, 060601 (2006).
- [4] A. Kitaev and J. Preskill, *Phys. Rev. Lett.* **96**, 110404 (2006).
- [5] M. Levin and X. G. Wen, *Phys. Rev. Lett.* **96**, 110405 (2006).
- [6] H. Li and F. D. M. Haldane, *Phys. Rev. Lett.* **101**, 010504 (2008).
- [7] M. Haque, O. Zozulya, and K. Schoutens, *Phys. Rev. Lett.* **98**, 060401 (2007);
- [8] O. S. Zozulya, M. Haque, K. Schoutens, and E. H. Rezayi, *Phys. Rev. B* **76**, 125310 (2007).

- [9] S. Dong, E. Fradkin, R. G. Leigh and S. Nowling, JHEP05 (2008) 016.
- [10] O. Zozulya, M. Haque, and N. Regnault; Phys. Rev. B **79** 045409 (2009).
- [11] N. Regnault, B. A. Bernevig, and F. D. M. Haldane, Phys. Rev. Lett. **103**, 016801 (2009).
- [12] A. G. Morris and D. L. Feder, Phys. Rev. A **79**, 013619 (2009).
- [13] A. M. Läuchli, E. J. Bergholtz, J. Suorsa, and M. Haque, Phys. Rev. Lett., **104**, 156404 (2010).
- [14] R. Thomale, A. Sterdyniak, N. Regnault, and B. A. Bernevig, Phys. Rev. Lett. **104**, 180502 (2010).
- [15] P. Fendley, M. P. A. Fisher, and C. Nayak, J. Stat. Phys. **126**, 1111 (2007).
- [16] B. A. Friedman and G. C. Levine, Phys. Rev. B **78**, 035320 (2008).
- [17] S.R. White, Phys. Rev. Lett. **69**, 2863 (1992); Phys. Rev. B **48**, 10345 (1993).
- [18] U. Schollwöck, Rev. Mod. Phys. **77**, 259 (2005), and references therein.
- [19] F. Verstraete and J. I. Cirac, arXiv:cond-mat/0407066; F. Verstraete, M. M. Wolf, D. Perez-Garcia, and J. I. Cirac, Phys. Rev. Lett. **96**, 220601 (2006).
- [20] G. Vidal, Phys. Rev. Lett. **101**, 110501 (2008).
- [21] N. Shibata and D. Yoshioka, Phys. Rev. Lett. **86**, 5755 (2001); J. Phys. Soc. Jpn. Vol.**72**, 664 (2003); N. Shibata, Prog. Theor. Phys. Suppl. No. 176 (2008) 182.
- [22] E.J. Bergholtz, *Density Matrix Renormalization Group Analysis of Spin Chains and Quantum Hall Systems*, Diploma thesis (Stockholm University, 2002).
E. J. Bergholtz and A. Karlhede, arXiv:cond-mat/0304517.
- [23] A. E. Feiguin, E. Rezayi, C. Nayak, and S. Das Sarma, Phys. Rev. Lett. **100**, 166803 (2008).
- [24] D. L. Kovrizhin, Phys. Rev. B **81**, 125130 (2010).
- [25] C. Castelnovo and C. Chamon, Phys. Rev. B **76**, 184442 (2007).
- [26] C. Castelnovo and C. Chamon, Phys. Rev. B **77**, 054433 (2008).
- [27] A. Hamma, W. Zhang, S. Haas, and D. A. Lidar, Phys. Rev. B **77**, 155111 (2008)
- [28] S. Iblisdir, D. Pérez-García, M. Aguado, and J. Pachos, Phys. Rev. B **79**, 134303 (2009).
- [29] S. Furukawa and G. Misguich, Phys. Rev. B **75**, 214407 (2007).
- [30] S. Papanikolaou, K. S. Raman, and E. Fradkin, Phys. Rev. B **76**, 224421 (2007).
- [31] D. Gioev and I. Klich, Phys. Rev. Lett. **96**, 100503 (2006).
M. M. Wolf, Phys. Rev. Lett. **96**, 010404 (2006).
E. Fradkin and J. E. Moore, Phys. Rev. Lett. **97** (2006) 050404.
T. Barthel, M. C. Chung and U. Schollwöck, Phys. Rev. A **74**, 022329 (2006).
W. Li, L. Ding, R. Yu, T. Roscilde, and S. Haas, Phys. Rev. B **74**, 073103 (2006).
L. Ding, N. Bray-Ali, R. Yu, and S. Haas, Phys. Rev. Lett. **100**, 215701 (2008).
R. Yu, H. Saleur, and S. Haas, Phys. Rev. B **77**, 140402(R) (2008).
B. Hsu, M. Mulligan, E. Fradkin, and E. Kim, Phys. Rev. B **79**, 115421 (2009).
N. Bray-Ali, L. Ding, and S. Haas, Phys. Rev. B **80**, 180504 (2009).
L. Tagliacozzo, G. Evenbly, and G. Vidal, Phys. Rev. B **80**, 235127 (2009).
- [32] I. D. Rodriguez and G. Sierra, Phys. Rev. B **80**, 153303 (2009).
- [33] E. J. Bergholtz and A. Karlhede, Phys. Rev. Lett. **94**, 026802 (2005); J. Stat. Mech. L04001 (2006); Phys. Rev. B **77**, 155308 (2008); E. J. Bergholtz, T. H. Hansson, M. Hermanns, and A. Karlhede, Phys. Rev. Lett. **99**, 256803 (2007); E. J. Bergholtz, T. H. Hansson, M. Hermanns, A. Karlhede, and S. Viefers, Phys. Rev. B **77**,165325 (2008) .
- [34] F. D. M. Haldane, Phys. Rev. Lett. **51**, 605 (1983).
- [35] S. A. Trugman and S. A. Kivelson, Phys. Rev. B **31**, 5280 (1985).
- [36] R. B. Laughlin, Phys. Rev. Lett. **50**, 1395 (1983).
- [37] A. Seidel, H. Fu, D. -H. Lee, J. M. Leinaas, and J. Moore, Phys. Rev. Lett. **95**, 266405 (2005).
- [38] P. W. Anderson, Phys. Rev. B **28**, 2264 (1983).
- [39] R. Tao and D. J. Thouless, Phys. Rev. B **28**, 1142 (1983).
- [40] E. H. Rezayi and F. D. M. Haldane, Phys. Rev. B **50**, 17199 (1994).
- [41] N. Read, Phys. Rev. B **79**, 045308 (2009).
- [42] F. D. M. Haldane, arXiv:0906.1854v1.

- [43] A. Seidel, Phys. Rev. Lett. **101**, 196802 (2008); arXiv:1002.2647v1.
- [44] E. H. Rezayi, F. D. M. Haldane, and Kun Yang, Phys. Rev. Lett. **83**, 1219 (1999).
- [45] K. Yang, F. D. M. Haldane, and E. H. Rezayi, Phys. Rev. B **64**, 081301(R) (2001).
- [46] G. Vidal, J. I. Latorre, E. Rico and A. Kitaev, Phys. Rev. Lett. **90**, 2279021 (2003).
- [47] M. B. Hastings, J. Stat. Mech. (2007) P08024.
- [48] E. J. Bergholtz and A. Karlhede, J. Stat. Mech. (2009) P04015.
- [49] P. K. Lam and S. M. Girvin, Phys. Rev. B **30**, 473 (1984).
- [50] M. Hermanns, J. Suorsa, E. J. Bergholtz, T. H. Hansson, and A. Karlhede, Phys. Rev. B **77**, 125321 (2008).
- [51] J. K. Jain, Phys. Rev. Lett. **63**, 199 (1989).